OE Optical Engineering

RESEARCH PAPER

Fiber bundle-based beam tracking approach for free space optical communications link optimization

Krunal Patel,* Michelle O'Toole, Katherine Newell, Radha Venkat, and Hala Tomey

The Johns Hopkins University Applied Physics Laboratory, Laurel, Maryland, United States

ABSTRACT. A robust pointing, acquisition, and tracking approach is critical to closing and maintaining a free space optical communications link. Many fiber-coupled terminal architectures use a beamsplitter to direct a portion of the received light onto a quadrant detector and generate an error signal. A feedback control loop uses this error signal to adjust a fine steering element to maximize power into the collection fiber. However, this approach produces additional insertion loss due to transmission through a beamsplitter and tracking loss due to inevitable boresighting errors between the quadrant detector and the collection fiber. We present an alternative architecture that makes use of a hexagonally packed, seven-fiber bundle for data beam tracking. The outer fibers are inherently co-boresighted position sensors used to sense displacement of the received beam from the central data fiber. We present field test data directly comparing performance between a fiber bundle-based terminal and a quadrant detector-based terminal. Our results show nearly an order of magnitude of improvement in control loop tracking stability and a 2.8× improvement in tracking performance as seen in Strehl ratio for the fiber bundle system.

© The Authors. Published by SPIE under a Creative Commons Attribution 4.0 International License. Distribution or reproduction of this work in whole or in part requires full attribution of the original publication, including its DOI. [DOI: 10.1117/1.OE.63.4.041212]

Keywords: free space optics; beam tracking; fiber bundle; optical communications

Paper 20230759SS received Aug. 15, 2023; revised Feb. 23, 2024; accepted Feb. 24, 2024; published Mar. 18, 2024.

1 Introduction

Free space optical (FSO) communications systems offer many advantages over traditional radio frequency communications links. FSO links can be operated from a variety of wavelength bands in the nanometer and micron regime to enable greater bandwidth and reduced signal interference compared to radio links. This article will focus specifically on the optical C-band (1530 to 1565 nm). FSO link designs vary according to the intended applications and take on many forms depending on the network topology, bandwidth needs, and link environment.[1–3]

FSO systems consist of a transceiver backend to transmit and receive data that has been modulated onto an optical carrier as well as a free space terminal frontend to direct outgoing light through an aperture and incoming light onto a detector. Many multi-Gbit/s data rate FSO systems have been implemented with a fiber-coupled detector in the optical terminal.[4,5] Optical fibers coupled with receiver modules offer a very sensitive detection option for multi-Gbit/s systems and provide an added opportunity to optically preamplify the received signal to improve link margin. These systems have been successfully demonstrated to provide robust links when coupled with a beam tracking architecture that can maximize the optical power entering the

*Address all correspondence to Krunal Patel, krunal.patel@jhuapl.edu

receive fiber. Some of these systems use an optical beam splitting method in which one path receives data via a fiber receiver module and the other path provides beam tracking using a set of four colocated optical sensors referred to as a quadrant detector.[6] However, this method can result in added insertion loss and present alignment challenges. In this article, we will present a rethinking of this tracking approach that uses seven co-boresighted fibers in a fiber bundle design in which the outer six fibers serve as tracking sensors and the central fiber serves as a data beam receiver.

In Sec. 2 of this article, we will discuss common FSO beam tracking architectures using adaptive optics (AO) mirrors as beam direction components and optical sensors for beam tracking. In Sec. 3, we will discuss the fundamental challenge imposed by thermal expansion in a beamsplitter architecture that separately receives data in a fiber-coupled terminal and tracks an incoming beam on a quadrant detector. In Sec. 4, we will discuss the benefits of using a hexagonally packed, seven-fiber bundle as a co-boresighted position sensor and receiver in place of a quadrant detector. In Sec. 5, we will discuss field test results demonstrating nearly an order of magnitude improvement in control loop tracking stability and a 2.8× improvement in tracking performance as seen in Strehl ratio between the common quadrant detector approach and the presented fiber bundle approach. In Sec. 6, we will conclude with a summary of key takeaways.

2 Beam Detection and Tracking Overview

Atmospheric turbulence can be detrimental to beam detection, tracking, and ultimately coupling to the receive fiber for FSO links when operating close to Earth's surface. The resulting beam propagation close to the ground or over water creates a coherence breakdown, resulting in a nonuniform distribution across a beam profile.[7] Beam wander and optical scintillation encountered during beam propagation produce a time-varying beam spot on the receiver plane and a highly variable received power distribution, as illustrated qualitatively in Fig. 1.[8,9] Beam wander shifts the transmitting beam around at a subhertz level while received power fluctuations due to scintillation can occur at up to kilohertz levels. The combined effect creates a received power distribution similar to Fig. 1(c) with a receiver plane mapping similar to Fig. 1(d).

The fluctuating received power distribution is a result of the dynamic beam position seen at the face of the optical terminal. Consequently, one of the most significant FSO design challenges is developing the pointing, acquisition, and tracking (PAT) system to consistently mitigate beam wander and scintillation effects and stabilize the received power distribution. The PAT system keeps a directional FSO data beam precisely aligned between communications nodes by providing continuous feedback control of the incoming light to maximize the amount of power incident on an optical receiver. PAT designs often use a gimbal for coarse beam steering to enter the field of regard of the opposing optical terminal in a point-to-point communications link. A fine beam steering approach is then used to focus and direct collected light through an aperture to an FSO communications receiver via lenses and beam steering optics.[10]

FSO receivers placed at the focus of the collected light come in many forms. A few of the most common FSO receivers include single-mode fibers (SMFs) coupled with fiber receiver modules, avalanche photodiodes (APDs), and P-I-N (PIN) photodiodes. Each receiver has its benefits and drawbacks depending on the given application, as detailed in Table 1. An SMF receiver offers the opportunity to leverage telecommunications industry developments that rely

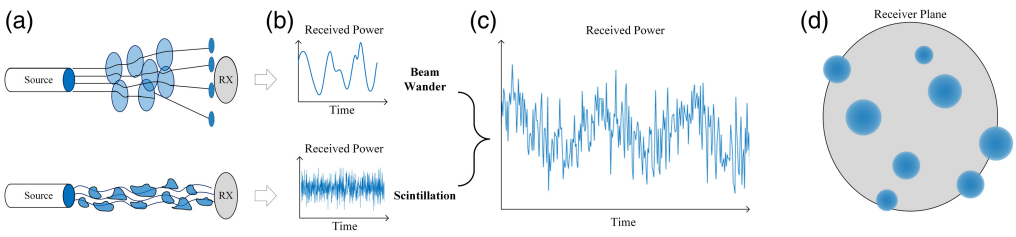

Fig. 1 Effects of beam wander and scintillation on received power showing (a) depictions of beam propagation due to beam wander and scintillation, (b) the individual effects on the received power distribution seen at an FSO terminal, (c) the combined effect of beam wander and scintillation on received power, and (d) the combined effect of beam wander and scintillation at the receiver plane.

Table 1 Detection type summary.

Detection type	Error-free sensitivity at 10 Gbit/s (photons per bit)	Receiver diameter
Preamplified SMF	~7 – 193	Micron-wide
APD	~1000	Hundreds of Microns-wide
PIN	~6200	Millimeter-wide

on SMF. Signals received on an SMF can be optically preamplified to boost signal power and make significant gains in receiver sensitivity with minimal noise additions. However, SMF systems present a difficult PAT challenge due to the ultraprecise pointing accuracy required to successfully couple light into an SMF core that is on the order of microns in diameter.[11] Alternatively, an APD offers a wider field of view with a detector diameter of up to hundreds of microns, resulting in a less-constrained pointing requirement.[12] Signals received on an APD can be electrically preamplified but at the cost of adding excessive noise to the received signal. APDs inherently experience excess dark noise and shot noise, limiting their capacity for sensitivity improvements. PIN photodiodes do offer relaxed pointing requirements with up to millimeter detector diameters,[13] but they also tend to be greatly limited in sensitivity because of high inherent noise.

When examining high-capacity, error-free links at a 10 Gbit/s data rate, the required receiver sensitivities for optically preamplified SMF receivers can range from ~7 to 193 photons per bit depending on the implementation.[14] Meanwhile, PIN photodiodes require ~6200 photons per bit, and APDs require ~1000 photons per bit to achieve an error-free 10 Gbit/s data rate. Developments in APD technology for FSO systems as seen in Ref. 4 facilitate using APD arrays for simultaneous, colocated beam sensing and communication detection to provide links that are robust to atmospheric turbulence while having simplified tracking architectures. However, these APD designs become limited in performance when approaching the sensitivities required for multi-Gbit/s rates.

To enable sensitive detection via SMF technologies, detection hardware must be paired with an effective beam tracking system to receive Gbit/s data rates error-free. Common tracking architectures for an FSO terminal use varying degrees of AO to overcome atmospheric aberrations and optimize power on the receiver. First-order AO correction of tip/tilt movement seen in the beam can be achieved using a fast steering mirror (FSM) with a control bandwidth equal to or greater than the Greenwood frequency.[15] Beam position information is collected on a quadrant detector, and a controller computes an error signal from this information. The controller then sends a feedback correction to the FSM to adjust the mirror angle and direct light onto the receive detector.

Higher-order AO corrections beyond tip/tilt, such as focus, coma, and astigmatism corrections, allow the propagated beam to achieve greater degrees of recollimation in the optical terminal.[16] In these systems, a deformable mirror consisting of a continuous phase plate with several push/pull actuators is fed control information from a wavefront sensor or turbulence-tracking camera to correct for phase changes across the beam surface. Although this approach can add link margin to FSO links experiencing atmospheric beam breakup,[17] higher-order AO systems tend to be exceedingly complex and add notable size, weight, and power to a terminal when compared with the FSM and quadrant detector approach.

3 Impact of Co-Boresighting Errors on Data Beam Tracking

A robust PAT system for an FSO terminal relies on accurate boresighting between the receive fiber and the beam detector. In this section, we discuss the impact of separate optical paths on system boresighting to highlight the advantages of a co-boresighted system. A simplified example FSO system with a quadrant detector-based tracking approach is illustrated in Fig. 2. In this monostatic example, light is received through an optical telescope assembly and steered onto a collection fiber using an FSM. A 90/10 beamsplitter directs 10% of the incoming light onto a quadrant detector. A free space spectral filter is placed on the quadrant detector lens assembly to

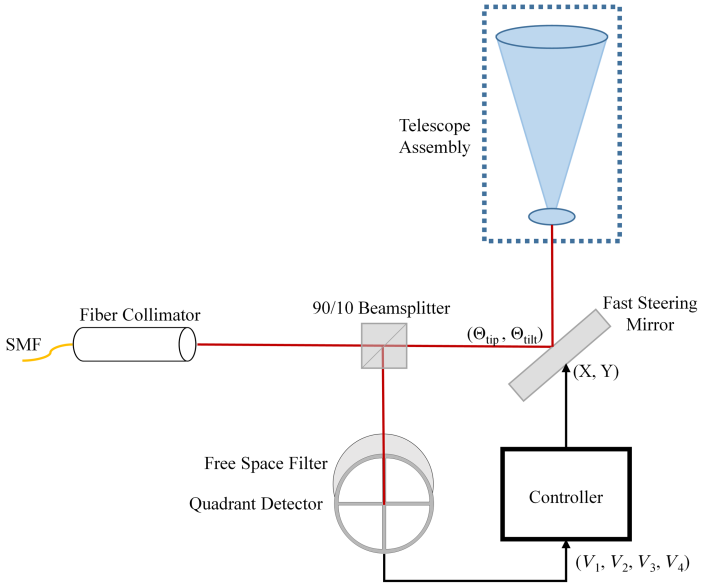

Fig. 2 Example FSO system using the quadrant detector beam tracking approach for fine data beam control.

provide necessary isolation between the outgoing and incoming beams, which are separated in wavelength. This scheme provides a feedback signal to the FSM through the system controller. The beamsplitter in the primary optical path results in 1 dB of additional system insertion loss. In a perfectly aligned and boresighted system, when the incoming light is centered on the quadrant detector, it will also be centered on the fiber collimator for optimal coupling of the data onto the fiber. A common approach to correcting for errors in beam position is to use voltage outputs from each quadrant, convert the outputs from analog to digital data, and have a real-time controller read the data. The real-time controller converts the optical power in the quadrants to Cartesian coordinates via voltage differentials to determine the pointing error, as shown in Fig. 3 and Eqs. (1)–(5). The Cartesian coordinates represent the incoming beam position on the face of the quadrant detector. The incoming beam coordinates are compared against the desired beam position to generate an error signal. The real-time controller subsequently sends a voltage correction proportional to the error signal to the FSM to induce an angular change in the FSM. The controller leverages a known relationship between FSM control voltage and angular beam position to shift the incoming beam to the desired position.

Figure 3 illustrates how optical power incident on the quadrant detector is converted to a Cartesian coordinate to represent beam position. Incoming light first couples to the detectors in the quadrant. Logarithmic amplifier electronics are used to convert the optical power to voltage levels. Each quadrant detector voltage is then weighted and summed together to create Cartesian coordinates. Equations (1)–(5) show the computation procedure in which V_n is the individual

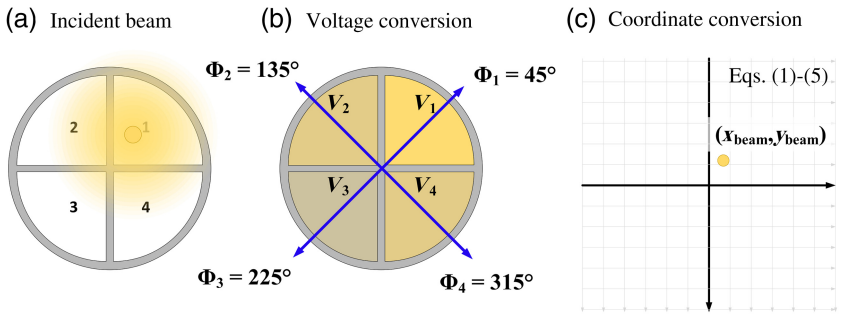

Fig. 3 Optical power to coordinate conversion. (a) Incoming light is incident on the quadrant detector face. (b) The optical power detected on each quadrant is converted to voltages. (c) The weighted sum of the quadrant voltages is computed to create a Cartesian coordinate.

detector voltage, k is the total number of detectors, V_{sum} is the sum of all the detector voltages, Φ_n is the angle of the detector placement, and x_n and y_n are the weighted detector voltages. The normalized Cartesian coordinate is the sum of all the weighted detector voltages, represented here as $(x_{\text{beam}}, y_{\text{beam}})$. The detector placement angles are used as weighting factors for beam position computation for both axes. For the quadrant detector, all four detectors are spaced at 90 deg apart from one another with respect to the x and y axes. The 90 deg separation trigonometry allows for equal weighting of each detector voltage and simplifies beam position calculation for the quadrant detector

$$V_{\text{sum}} = \sum_{n=1}^{k} V_n, \tag{1}$$

$$x_n = \frac{V_n * \cos(\Phi_n)}{V_{\text{sum}}}, \tag{2}$$

$$y_n = \frac{V_n * \sin(\Phi_n)}{V_{\text{sum}}}, \tag{3}$$

$$x_{\text{beam}} = \sum_{n=1}^{k} x_n, \tag{4}$$

$$y_{\text{beam}} = \sum_{n=1}^{k} y_n. \tag{5}$$

The quality of the co-boresighting between the data collection fiber and the beam tracking mechanism in an FSO system has a notable impact on tracking capability. As discussed in Ref. 18, fiber positioning error in the presence of atmospheric turbulence can reduce coupling efficiency onto an SMF. This error can be expressed in terms of three error types: lateral offset, focal offset, and tip/tilt offset. The fiber bundle tracking architecture introduced in this paper aims to reduce positioning error through the elimination of path differences between the detector and the fiber collimator that can cause varying degrees of these error types to occur.

Lateral and tip/tilt offset errors that occur during alignment can be fixed by adding final boresighting control in the FSM controller. A user-defined setpoint could allow for correction of alignment errors by directing the FSM to the (0,0) position when the quadrant detector is reading in light at a setpoint (X, Y) slightly offset from (0,0). However, as noted in Ref. 19, thermal expansion produces displacement in the alignment between the receive fiber and the quadrant detector. Thermal expansion is not static, and therefore its effects cannot be corrected by a simple calibration. In Fig. 4, we evaluate a simplified example of how thermal expansion might impact a system with separate paths between the detector and fiber collimator. If the beamsplitter experiences a slight tip/tilt misalignment due to thermal expansion, the incident angle of the incoming light onto the beamsplitter will change, translating to a positional error on one axis of the quadrant detector. This effect produces an error in the steering mirror controls and ultimately results in suboptimal positioning of the light onto the data fiber.

To explore the results of this error, we consider that the SMF detector has a core radius of 8.2 μm[20] and evaluate the limits of positional error that would cause the incoming light to miss the core of the fiber. The maximum tolerable full angle error before missing the core $\Theta_{\text{error, max}}$ is related to the core size of the fiber r and the optical path length d between the FSM and the fiber collimator as

$$\Theta_{\text{error, max}} \leq \tan^{-1}\frac{r}{d}. \tag{6}$$

Given an assumed optical path $d = 15$ cm, the maximum tolerable half angle pointing error is 27.3 μrad, suggesting that thermally induced angular errors of <1/500th of a degree can have large consequences for this system. Although this example has been simplified for the purpose of illustration, path differences between the detector and fiber collimator create opportunities for thermal expansion to introduce errors into the pointing and tracking system. Atmospheric turbulence already creates the need for actively tracked beams. Therefore, additional error

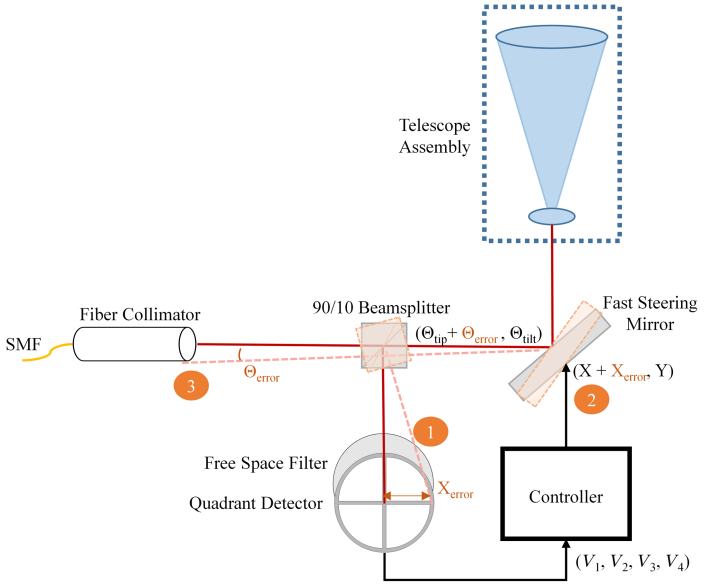

Fig. 4 Simplified example of how thermal expansion can affect system alignment where path differences exist between the fiber collimator and tracking detector. (1) Beamsplitter misalignment due to thermal expansion will produce a lateral offset error on the quadrant detector (2), which leads to incorrect information being sent to the FSM, resulting in (3) an angular pointing error for the light being directed onto the collimator.

introduced into this stringent pointing requirement poses challenges in efficiently coupling light from the free space channel onto the fiber.

While reducing the optical path length or engineering the optical payload frame to reduce the effects of thermal expansion are two potential ways to mitigate these effects, colocating the position sensor and the data fiber could reduce thermal expansion-induced displacement errors in the pointing and tracking system altogether. Devices exist that allow a fiber to be placed at the center of a quadrant detector, such as in Ref. 21, creating a common path between the tracking system and receive fiber. Although this approach would address lateral offset error, tip/tilt offset may still be a concern depending on how the fiber interfaces with the detector. Additionally, this approach poses a challenge in the case of a monostatic terminal design, in which the outgoing and incoming signals are separated in wavelength. As was seen in Fig. 3, a filter is placed on the lens assembly to direct light onto the quadrant detector to provide additional isolation between the high-power transmitted signal and the low-power received signal. With the colocation of the quadrant detector and the transmit/receive fiber, the free space filter would no longer be a viable option. Placing the fiber at the center of the quadrant detector would mean attenuating the outgoing transmitted signal as it passes through the filter in front of the quadrant detector. In the next section, we discuss the use of a fiber bundle as a co-boresighted tracking device that is more compatible with a monostatic terminal design.

4 Fiber Bundle as a Beam Position Sensor

A fiber bundle is a collection of fiber optical cables that have been packaged together into one cable. Fiber bundles have been demonstrated as sensors in various applications, such as medical imaging[22] and remote sensing.[23] Here, we demonstrate that a fiber bundle can be used as both a beam position sensor and a receive fiber in an FSO link, which provides the benefit of an inherent co-boresighting of the position sensor to the receive fiber.

Our system uses a seven-fiber bundle with a hexagonally packed structure, as shown in Fig. 5. The center fiber is an SMF with a numerical aperture of 0.14 that is connected to a backend modem for transmission and reception of the FSO data link. The outer six fibers are multi-mode fibers (MMFs) with numerical apertures of 0.22, providing wider acceptance angles compared with SMFs. The six outer fibers collect incoming stray light and are used to determine the pointing error of the received signal. Because of the precision manufacturing process of

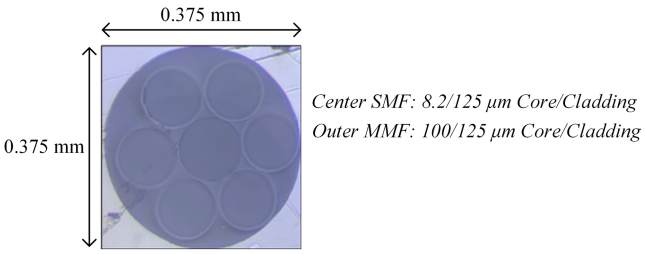

Fig. 5 Face of the fiber bundle captured through a fiber microscope, with the outer six 100-μm core MMFs designated as sensors and the center 8.2-μm core SMF designated as the data receiver.

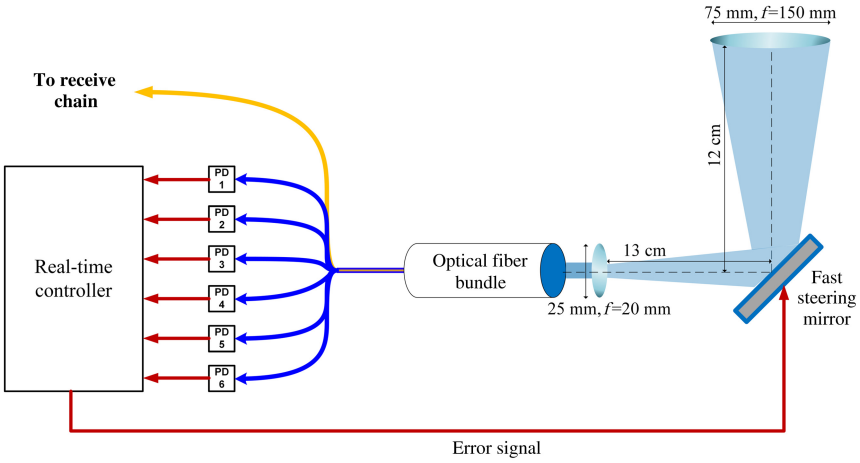

Fig. 6 High-level fiber bundle payload diagram.

the fiber bundle, the six MMFs are on the same focal plane as the data SMF. The co-alignment between the MMFs and SMFs is not affected by thermal expansion.

The fiber bundle is integrated into the FSO optical payload as shown in Fig. 6. The end of the fiber bundle that has all seven fibers packaged together is placed in the payload at the focal plane of the system. The six outer MMFs connect to 800 MHz bandwidth InGaAs photodiodes[24] to measure the received power for position sensing. The center fiber connects to a 10 Gbit/s optical receive chain for optical preamplification, filtering, and demodulation.

Analogous to the quadrant detector beam positioning approach, the outputs of the fiber position-sensing photodiodes are converted from analog to digital data and read by a real-time controller system. The real-time system uses the fiber bundle geometry to convert the optical power in the sensing fibers to Cartesian coordinates to determine the pointing error, as shown in Fig. 7. The Cartesian coordinates represent the incoming beam position on the face of the fiber

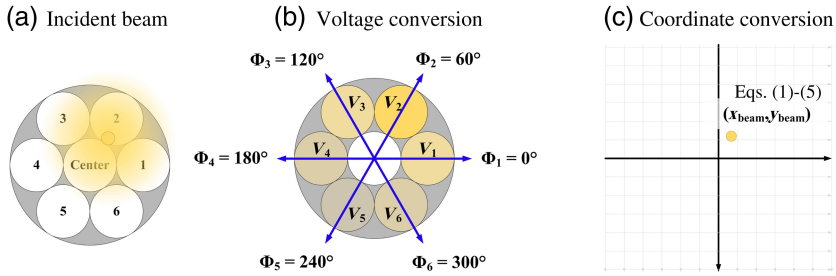

Fig. 7 Optical power to coordinate conversion. (a) Incoming light is incident on the fiber bundle face and coupled into the sensing fibers. (b) The optical power detected on each fiber is converted to a voltage and normalized based on the fiber's orientation angle. (c) The sum of the normalized fiber voltages is computed for each axis to create a Cartesian coordinate.

bundle. The computation process to obtain the coordinate is equivalent to that of the quadrant detector approach shown in Eqs. (1)–(5) except with $k = 6$ in place of $k = 4$. While the quadrant detector is arranged to have detectors spaced apart by 90 deg with respect to one another, the fibers in the fiber bundle are spaced 60 deg apart. Therefore, the voltages recorded from each fiber are not equally weighted, and the 60 deg separation trigonometry must be considered. This computation generates an error signal and a resulting proportional voltage correction that is sent to an FSM to correct the beam position and center the beam on the data receive fiber. Further details of this control method using a fiber bundle can be found in the patent in Ref. 25.

5 Field Test Results

In March 2019, we established an outdoor, 5 km FSO link between a 1 mm diameter quadrant detector terminal and the fiber bundle-based terminal described in Sec. 4. The link was maintained for 7–10 h each day of testing for 6 days in a desert environment, which included over 20°C fluctuation total in ambient temperature. During testing, data was recorded on the real-time controller system at 10 k Samples/s. The recording system logs power in the data receive fiber as well as the power on individual sections of the position sensor. The total power received on the data fiber is referred to as power in fiber (PIF), and the total power received on the position sensors is referred to as power in bucket (PIB). The tracking performance can be determined by computing the difference between PIF and PIB, referred to as the Strehl ratio, using

$$\text{Strehl Ratio (dB)} = \text{PIB (dBm)} - \text{PIF (dBm)}. \tag{7}$$

The position sensor location and the Strehl ratio were calculated for all data sets for both quadrant detector-based and fiber bundle-based terminals. The scatter plots in Fig. 8 show the position sensor locations recorded by the system during times when the system was optimized over the course of the test event. In previous field test events with the quadrant detector-based terminal, it was observed that to maintain a near-ideal Strehl ratio of −5 to 0 dB, the target position had to be continually optimized in the control system as temperature changed. To remove any data from times when the system was not optimized, any data points in which the Strehl ratio was below −5 dB were removed from the data in Fig. 8(a). Any data points in which the PIB was ≤ -30 dBm were removed from both data sets to remove outliers caused by line-of-sight blockages or deep link fades. Over this short link length, both terminals experienced similar environmental conditions, including Sun exposure, ambient temperature, and turbulence distribution. The temperature range recorded within the terminals corresponding to this data set spanned 19.8°C to 39.9°C. Turbulence measurements were also recorded on a scintillometer

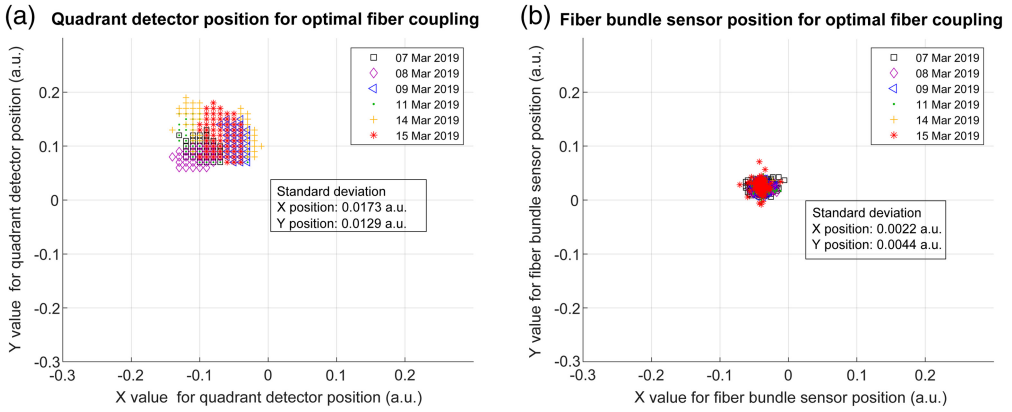

Fig. 8 Experimental position sensor setpoint distribution for (a) the quadrant detector and (b) the fiber bundle.

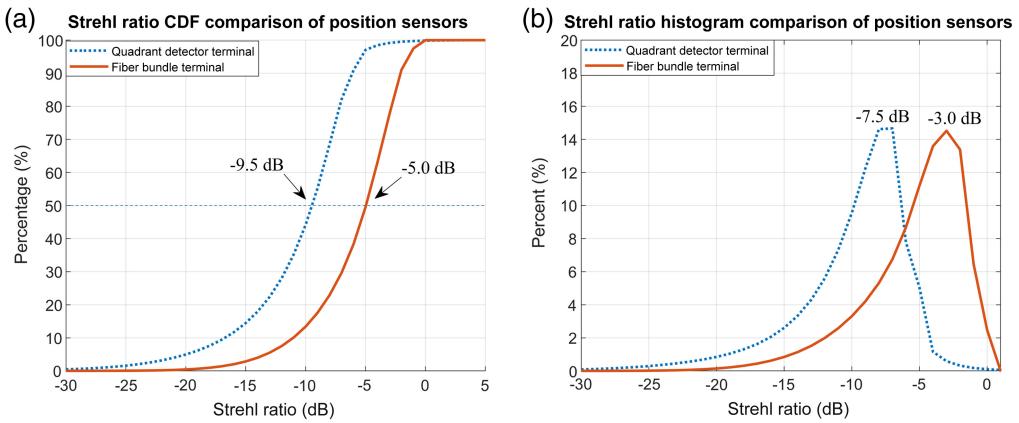

Fig. 9 Statistics comparison between quadrant detector-based and fiber bundle-based terminals using (a) Strehl ratio CDFs and (b) Strehl ratio histograms.

during the test, albeit not on the same optical path as the FSO link. The turbulence strength generally ranged between $C_n^2 = 5 \times 10^{-13}$ m$^{-2/3}$ and $C_n^2 = 5 \times 10^{-15}$ m$^{-2/3}$ during FSO link operation periods. The standard deviation of the optimal position sensor setpoint was computed for each terminal and is also shown in Fig. 8. The data show that the normalized position standard deviation for the fiber bundle was nearly an order of magnitude lower than that of the quadrant detector, demonstrating substantial improved tracking stability in the fiber bundle-based terminal over the quadrant detector-based terminal in the presence of large temperature variation. While the quadrant detector and fiber bundle sizes are different (1 mm diameter quadrant detector and 0.375 mm diameter fiber bundle), these results focus on the tracking stability of all the light that enters each detector regardless of detector size.

The overall tracking performance can be analyzed by viewing the cumulative distribution function (CDF) of the Strehl ratio for each system. The CDF shown in Fig. 9(a) was calculated for the entire testing period from March 7, 2019 to March 15, 2019. Data points in which a link outage had occurred were removed to prevent erroneous Strehl ratio calculations. The CDF shows that at the 50% point, the quadrant detector terminal Strehl as seen in the dotted line is −9.5 dB, and the fiber bundle terminal Strehl as seen in the solid line is −5.0 dB. This 4.5 dB tracking performance improvement represents a 2.8 factor gain, more than doubling the power coupled to the receive fiber in the fiber bundle-based terminal. Another way to analyze this data is to generate a histogram of the Strehl ratio, as presented in Fig. 9(b) using 1 dB wide bins. Looking at the peak of the histogram indicates the Strehl ratio that was most common for each system, with a most common Strehl of −7.5 dB for the quadrant detector terminal and −3.0 dB for the fiber bundle terminal. These results are consistent with the CDF-based assessment of a 4.5 dB tracking performance improvement.

6 Conclusion

The merits of a fiber bundle-based beam tracking scheme for FSO communications links are discussed. The challenges associated with a traditional beamsplitter and quadrant detector tracking method are evaluated, followed by a description of an architecture that eliminates the beamsplitter by using a fiber bundle paired with InGaAs photodiodes to provide fine data beam position information to an FSM that can optimize optical power incident on a receive fiber. Other advantages of the fiber bundle-based tracking approach are discussed, including guaranteed co-boresighting between tracking and data receive beam paths, compatibility with SMF preamplification to boost receiver sensitivity, and a wide acceptance angle to correct for alignment errors by using MMFs as tracking sensors. Data collected on a 5 km outdoor FSO link are presented along with an analysis showing nearly an order of magnitude of beam tracking stability improvement in changing thermal conditions and a 2.8× improvement in the Strehl ratio when using the fiber bundle-based beam tracking approach in place of the quadrant detector-based beam tracking approach.

Code and Data Availability

The data behind this article is available from the corresponding author upon reasonable request.

Acknowledgments

We thank our former colleagues, Juan Juarez and Lauren Weiss, for their valuable contributions.

References

1. S. A. Al-Gailani et al., "A survey of free space optics (FSO) communication systems, links, and networks," *IEEE Access* **9**, 7353–7373 (2021).
2. S. Chaudhary and A. Amphawan, "The role and challenges of free-space optical systems," *J. Opt. Commun.* **35**(4), 327–334 (2014).
3. F. Demers, H. Yanikomeroglu, and M. St-Hilaire, "A survey of opportunities for free space optics in next generation cellular networks," in *Ninth Annu. Commun. Networks and Serv. Res. Conf.*, Ottawa, Ontario, pp. 210–216 (2011).
4. W. S. Rabinovich et al., "Free-space optical communications research and demonstrations at the U.S. Naval Research Laboratory," *Appl. Opt.* **54**(31), F189–F200 (2015).
5. B. L. Edwards, "NASA's current activities in free space optical communications," *Proc. SPIE* **10563**, 105630X (2017).
6. J. C. Juarez et al., "Testing of a compact 10-Gbps Lasercomm system for maritime platforms," *Proc. SPIE* **10408**, 1040802 (2017).
7. L. C. Andrews and R. L. Phillips, *Laser Beam Propagation through Random Media*, SPIE Press, Bellingham, Washington (2005).
8. A. Trichili et al, "Roadmap to free space optics," *J. Opt. Soc. Am. B* **37**(11), A184–A201 (2020).
9. K. Kazaura et al., "Enhancing performance of next generation FSO communication systems using soft computing based predictions," *Opt. Express* **14**(12), 4958–4968 (2006).
10. Y. Kaymak et al., "A survey on acquisition, tracking, and pointing mechanisms for mobile free-space optical communications," *IEEE Commun. Surv. Tutor.* **20**(2), 1104–1123 (2018).
11. OFS, "Single-mode optical fiber geometries," https://www.ofsoptics.com/single-mode-optical-fiber-geometries (accessed 9 Aug. 9 2023).
12. Hamamatsu Photonics, "InGaAs APDs," https://www.hamamatsu.com/eu/en/product/optical-sensors/apd/ingaas-apd.html (accessed 9 Aug. 2023).
13. Hamamatsu Photonics, "InGaAs photodiodes," https://www.hamamatsu.com/eu/en/product/optical-sensors/photodiodes/ingaas-photodiode.html (accessed 9 Aug. 2023).
14. D. Caplan, "Laser communication transmitter and receiver design," *J. Opt. Fiber Commun. Rep.* **4**, 225–362 (2007).
15. R. K. Tyson and B. W. Frazier, *Field Guide to Adaptive Optics*, 2nd ed., SPIE Press, Bellingham, Washington (2012).
16. R. K. Tyson and B. W. Frazier, *Principles of Adaptive Optics*, 5th ed., CRC Press (2022).
17. C. Liu et al., "Performance evaluation of adaptive optics for atmospheric coherent laser communications," *Opt. Express* **22**(13), 15554–15563 (2014).
18. Y. Bian et al., "Free-space to single-mode fiber coupling efficiency with optical system aberration and fiber positioning error under atmospheric turbulence," *J. Opt.* **24**(2), 025703 (2022).
19. V. Mai and H. Kim, "Beaconless angle-of-arrival tracking with improved receiver sensitivity and tracking precision for free-space optical communications," *Opt. Commun.* **527**, 128963 (2023).
20. Corning, Inc., "Corning SMF-28e+ optical fiber: product information," PI1463, https://www.corning.com/media/worldwide/coc/documents/Fiber/product-information-sheets/PI1463_07-14_English.pdf (accessed July 2014).
21. OSI Optoelectronics, "SPOT-9D-0: annular quadrant silicon photodiode," Preliminary datasheet Rev. X1, https://osioptoelectronics.com/media/pages/products/photodetectors/backscatter-photodetectors/spot9d-0/4cab37dc01-1675100515/spot-9d-0-datasheet.pdf (accessed 9 Aug. 2023).
22. J. Sun et al., "Quantitative phase imaging through an ultra-thin lensless fiber endoscope," *Light Sci. Appl.* **11**, 204 (2022).
23. M. Yasin et al., "Fiber bundle sensor for detection of formaldehyde concentration in fish," *Opt. Fiber Technol.* **52**, 101984 (2019).
24. GPD Optoelectronics Corp., "High speed InGaAs photodiodes," GAP300 datasheet, GPD Optoelectronics Corp, Salem, New Hampshire, https://www.gpd-ir.com/wp-content/uploads/High-Speed-InGaAs-Photodiodes.pdf (accessed 9 Aug. 2023).
25. K. T. Newell et al., "Free-space optical terminal," U.S. Patent 10,763,961, filed August 31, 2019, and issued July 9 (2020).

Krunal Patel is a photonics systems engineer and manager of various free space optical communications projects at the Johns Hopkins University Applied Physics Laboratory. He received his bachelor's and master's degrees in electrical engineering from Drexel University in 2016. Since 2016, he has worked on the development of high-speed free space and fiber optical communications systems. His competencies include optical and electrical design and test of optical modems and terminals and integration into multilink networks.

Michelle O'Toole received her BS degree in physics from Lehigh University and her MS degree in applied physics from the Johns Hopkins University. She is a photonics engineer and supervisor of the optical communications section at the Johns Hopkins University Applied Physics Laboratory, focusing on the development of prototype photonic systems. Her experience includes optical communications and microwave photonics.

Katherine Newell is the supervisor of the Optics and Photonics Group at the Johns Hopkins University Applied Physics Laboratory. She received her bachelor's and master's degrees in electrical engineering at Bucknell University in 2011 and the Johns Hopkins University in 2015, respectively. Her career has focused on photonic systems engineering and the development of free space and fiber optical communications systems.

Radha Venkat is a software engineer at the Johns Hopkins University Applied Physics Laboratory. She received her bachelor's degree in applied physics from Case Western Reserve University in 1996 and her master's degree in electrical engineering from Princeton University in 1998. She has worked on projects involving photonics, free space and fiber optic communications systems, advanced sensor development, and weapons systems. Her competencies include instrumentation, data collection and analysis, control systems, and algorithm design.

Hala Tomey is an electronics packaging engineer in the Johns Hopkins University Applied Physics Laboratory's Research and Exploratory Development Department. She has a BS in mechanical engineering from Boston University and an MS in mechanical engineering from the University of Maryland, College Park. She works on mechanical design, analysis, and fabrication of electronics for space and military systems. She manages the design and fabrication of electro-optical systems and their integration in support of field testing.